J. Fluid Mech. (1994), vol. 275, pp. 257–283

Dynamics of three-dimensional coherent structures in a flat-plate boundary layer

By DIETMAR REMPFER[1] AND HERMANN F. FASEL[2]

[1]Institut für Aerodynamik und Gasdynamik, Universität Stuttgart, 70550 Stuttgart, Germany

[2]Department of Aerospace and Mechanical Engineering, The University of Arizona, Tucson, AZ 85721, USA

(Received 12 May 1993 and in revised form 31 March 1994)

An investigation is presented that analyses the energy flows that are connected to the dynamical behaviour of coherent structures in a transitional flat-plate boundary layer. Based on a mathematical description of the three-dimensional coherent structures of this flow as provided by the Karhunen–Loève procedure, energy equations for the coherent structures are derived by Galerkin projection of the Navier–Stokes equations in vorticity transport formulation onto the corresponding basis of eigenfunctions. In a first step, the time-averaged energy balance – showing the energy flows that support the different coherent structures and thus maintain the fluctuations of the velocity field – is considered. In a second step, the instantaneous power budget is investigated for the particularly interesting case of a coherent structure providing a prime contribution to the characteristic spike events of the transitional boundary layer. As this structure shows a strong variation in energy, the question about which mechanisms cause these variations is addressed. Our results show that the occurrence of a spike must be attributed to an autonomous event and cannot be interpreted as just an epiphenomenon of the passage of a Λ-vortex.

1. Introduction

Although organized motions in turbulent flows certainly could have been observed since the experiments of Reynolds (1883) near the end of the previous century, their existence has been largely ignored. It was not until the mid 1950's that the presence of coherent structures was discussed (Townsend 1956). The existence of these structures indicates that the description of turbulent flows as being in a state of unstructured turmoil is not exact. However, it was just this picture of a non-deterministic structure of the turbulent flow that led to the classical statistical description of turbulence.

While the statistical theory of turbulence did indeed provide the prime contribution to our current understanding of turbulence (see, for example, the textbook by Monin & Yaglom 1973), there are still many unanswered questions, leaving the entire subject far from being fully understood. One of the main problems – in fact, *the* main problem – of the statistical theory of turbulence, the well-known closure-problem, can be considered a consequence of the fact that this theory *per definitionem* cannot consider the detailed dynamics of the flow. As the Reynolds stresses are, in general, spatio-temporal functionals (and not functions) of the flow, neglect of the details of transient turbulent motion necessitates modelling these stresses in a situation of incomplete information.

However, as mentioned above, another view of turbulence, closely connected to the concept of 'coherent structures', gained attention about four decades ago (Townsend 1956). This coherent structure approach to turbulence is motivated by the idea that turbulent flows are not just fluids in a state of complete disorder and chaos. Rather, such flows are composed of the superposition of a number of organized motions, the so-called 'coherent structures'. An important implicit ingredient of this approach is the assumption – or hope – that there is only a comparably small number of such structures that are relevant to the essential dynamics of the flow. If this is true, then the investigation of the dynamics of these structures would be a feasible task, promising not only deeper insight into the 'nature' of turbulent flows, but also the possibility of gaining additional information for modelling purposes.

Since the work by Townsend, literally hundreds of papers have been written on the topic of coherent structures. Instead of attempting a general review of these, we refer the reader to the review articles by Cantwell (1981), Fiedler (1987), and Robinson (1991). Here, we will confine ourselves to pointing out a few of the contributions that are closely related to our subject.

Some of the first detailed investigations of the near-wall structures of turbulent boundary layers on a mainly phenomenological level were reported by Einstein & Li (1956) and Kline & Runstadler (1959). In the 1960's, further important contributions towards an understanding of the structures of turbulent flows followed, represented by, among others, the works of Runstadler, Kline & Reynolds (1963), Kline *et al.* (1967), and Kim, Kline & Reynolds (1971) of the Stanford group. These investigations confirmed the relevance of coherent structures to the dynamics of turbulent flows, particularly because of their important contribution to turbulence production and momentum transport in the turbulent boundary layer. However, it was not until the impressive flow visualizations by Brown & Roshko (1974) that the idea of coherent structures having a significant role in turbulent flows was finally established.

Important advances in the investigation of coherent structures took place at the end of the 1960's and in the beginning of the 1970's. In particular, progress was made in the formulation of explicit definitions of the term 'coherent structure' and the development of corresponding, widely accepted methods to determine these structures. There were essentially two different approaches. One of these approaches can be traced back to investigations by Gupta, Laufer & Kaplan (1971), Wallace, Eckelmann & Brodkey (1972), and Willmarth & Lu (1972). These authors introduced the techniques of *conditional sampling* or *phase averaging* to determine coherent structures. Detailed accounts of the development and results of these methods are given by Hussain (1983, 1986). The biggest difficulty with these techniques results from the fact that they require the researcher to already have an idea of some characteristic properties of the structure to be determined. Based on that, a criterion for the detection of this structure is developed that allows one to choose, from a set of data or flow visualizations of a flow field, all those realizations that meet the criterion. By an appropriate averaging of the selected flow fields, the prototypical coherent structure can be obtained. The main drawback of the methods based on conditional sampling are obvious in that the results depend strongly on the choice of criteria for the coherent structure. This choice, in turn, requires that information on the coherent structures be present before they are actually known. Thus, there is actually no fixed, *a priori* definition present at the base of techniques using conditional sampling. This is, of course, a serious disadvantage, since we think that the notion of a coherent structure is of little use as long as it is not possible to give a precise, quantitative

description of the role such structures play in the flow. Such a description, however, requires an exact definition and a mathematical description of the coherent structures.

These criteria are met by a method that has been proposed by Lumley (1967). He suggested a technique based on the Karhunen–Loève expansion from probability theory (Loève 1955) that is now known as *proper orthogonal decomposition* (POD). It has the advantage of completely eliminating the need for any kind of external information or prior knowledge concerning the structures to be identified. For our investigation, we used the POD method to identify the coherent structures. A fairly complete account of this method is given by Lumley (1970), and several advanced topics are treated in a series of papers by Sirovich (1987) and in a recent review paper by Berkooz, Holmes & Lumley (1993). For a short review of works using this method, we refer the reader to Rempfer & Fasel (1994).

The purpose of this investigation is to obtain a deeper understanding of the dynamics of coherent structures in a transitional flat-plate boundary layer. The data base available for our investigations was obtained from a direct numerical simulation of the three-dimensional, spatial evolution of a transitional flat-plate boundary layer (see §2). The physical domain considered here is composed of a certain stage of the transition process where a highly nonlinear evolution of Tollmien–Schlichting waves has set in and where the characteristic spike stages during breakdown to turbulence occur. Our emphasis on the transitional boundary layer has been dictated by current limitations in the simulation of spatially evolving turbulent flows. Owing to the need for long integration domains in the streamwise direction and requirements for resolution, direct numerical simulations (DNS) of fully developed turbulence are extremely expensive using currently available computers. The transitional boundary layer, on the other hand, is an interesting research topic *per se*. In addition, because of numerous analogies of transitional boundary layers to fully turbulent boundary layers (see, for example, Blackwelder 1983 and Rempfer & Fasel 1994), our work may also shed some light on open questions concerning fully turbulent flows.

So the motivation for the investigations presented here was to gain deeper insight into the mechanisms behind the dynamical behaviour of coherent structures in transitional boundary layers. In our previous investigation (Rempfer & Fasel 1994) we have shown that the dynamical coherent structures of the flat-plate boundary layer can be described by pairs of eigenfunctions that contain complete information on the spatial evolution of the structures. We also demonstrated that by considering coherent structures as described by such pairs of eigenfunctions, one can obtain a compact description of the complex phenomena occurring in the transitional boundary layer. While in our previous work we thus mainly focused on phenomenological aspects of the behaviour of coherent structures in our flat-plate boundary layer, we now want to emphasize the causality behind the scene. In other words, with the present paper we leave the kinematics of coherent structures described in our previous paper, and we now turn to the dynamics of these entities. Towards this end, we will proceed in two steps. In the first step, we investigate the time-averaged energy budget of the coherent structures, which yields information on the energy flows that support the different coherent structures and thus maintain fluctuations in the boundary layer. In the second step we look in detail at the instantaneous energy flows that are responsible for the dynamical interactions between different structures and the base flow. In particular, we will show, for an especially interesting case – that of a structure being responsible for the well-known spike signals of transition – which mechanisms are responsible for formation and decay of such a structure. Thus with this second step, we are addressing the first of the two generic questions concerning wall layers that

were raised (but excluded) by Aubry *et al.* (1988): *'Where do the coherent structures in the wall region come from, i.e., what dynamical mechanism is responsible for their life cycle?'*

A brief description of the numerical simulation that provided our data base is given in §2. Section 3 is devoted to the dynamical equations for the coherent structures, starting with a brief review of some of the properties of the Karhunen–Loève eigenfunctions as provided by the POD method. After the derivation of the energy equations, a detailed interpretation of the terms making up this equation will be given. In §4, some of the properties of the structures that are treated in later sections are discussed to assist in mental visualization of the problem. Sections 5 and 6, which form the main body of this paper, contain a thorough investigation of the time-averaged and the instantaneous energy flows, respectively.

2. Data base

The investigations discussed here are based on data obtained from a direct numerical simulation of an experiment by Kachanov *et al.* (1985) on controlled transition in a flat-plate boundary layer. A first version of this simulation was carried out by Rist & Fasel (1994), who achieved very good agreement between calculation and experiment up to the multi-spike stages of transition. At these stages, slight deviations from periodicity are already breaking the temporal symmetry of the imposed boundary conditions, indicating the onset of turbulence. The actual data used for the work reported here are from a repetition of the above simulation using improved resolution in all spatial directions as well as in time (Kloker 1993).

The simulations by Rist & Fasel (1994) and by Kloker (1993) were based on the so-called spatial model, which allows study of the spatial evolution of a periodically disturbed, incompressible flat-plate boundary layer. The integration domain used in the simulation and the corresponding coordinate system are shown in figure 1. The numerical method used for these simulations employed finite differences in the streamwise and wall-normal (x- and y-) coordinates while the spanwise coordinate was discretized in function space using Fourier modes. For a more detailed discussion of the numerical method and, in particular, the boundary conditions used, see Kloker (1993), and Kloker, Konzelmann & Fasel (1993). Within the domain considered here, the finite-difference resolutions in wall units were better than $\Delta x^+ = 5$ in the streamwise direction and $\Delta y^+ = 3$ in the wall-normal direction. For the spanwise direction, only 16 (aliasing-free) Fourier modes were present. Thus, mainly owing to the limited number of Fourier modes, the grid used in the simulation was not sufficient to resolve the flow up to regions of fully developed turbulence. The results were reliable only up to a distance of about 500 mm from the leading edge, which corresponds to a Reynolds number based on momentum thickness of $Re_{\delta_2}^{max} = 575$.

For the simulation of the experiments on controlled transition by Kachanov *et al.* (1985), Rist & Fasel (1994) introduced disturbances via their boundary condition for the wall-normal (v-) velocity component. This boundary condition simulated periodic suction and blowing within a narrow strip (oriented normal to the flow direction) on the flat plate. As in the experiments, these disturbances are periodic in time and symmetric with respect to the (x, y)-plane. As the Navier–Stokes equations preserve such symmetries, Rist & Fasel were able to restrict their simulation to flow fields that are likewise symmetric with respect to the (x, y)-plane. Some further implications of this restriction, particularly concerning the application of POD to such flow fields, were discussed by Rempfer & Fasel (1994). In short, this symmetry

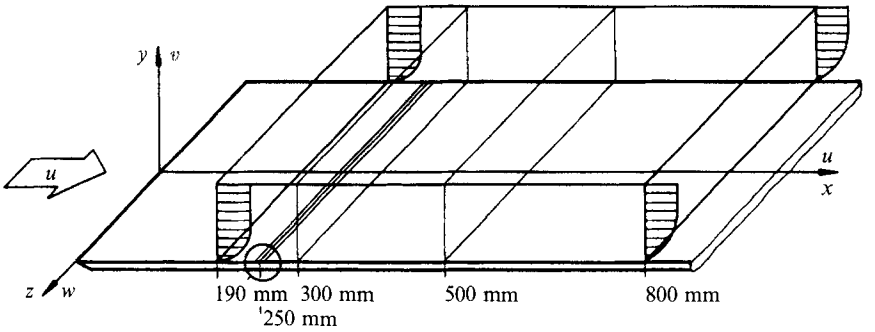

FIGURE 1. Integration domain of numerical simulation by Rist & Fasel (1994).

assumption leads to the flow fields not being homogeneous in the spanwise direction. Therefore, our eigenfunctions cannot be factored into products of some function of x and y and simple sinusoids for the spanwise direction, but describe fully three-dimensional structures.

In the investigations reported here, we confined ourselves to a small subregion of the integration domain. While the integration domain of the simulation covered the flat plate in the range $190\,\text{mm} \leqslant x \leqslant 800\,\text{mm}$, this region extends from a streamwise distance of about $x = 403\,\text{mm}$ from the leading edge of the flat plate up to about $x = 450\,\text{mm}$. Within this range, the spike stages of transition up to the three-spike stage can be observed. The region is about 8.77 mm in the wall-normal direction, which corresponds to 2.5 boundary-layer thicknesses, and 24.5 mm in the spanwise direction. Using a free-stream velocity of $9.09\,\text{m}\,\text{s}^{-1}$, the Reynolds number based on momentum thickness can be calculated as $Re_{\delta_2}^{max} = 340$ at the upstream and $Re_{\delta_2}^{max} = 460$ at the downstream boundary. The dimensions of the region in wall units are $\Delta x^+ = 1600$, $\Delta y^+ = 288$, and $\Delta z^+ = 805$. The ensemble of flow fields used in this work consisted of 440 equally spaced time steps within one time period of the imposed disturbances. The region investigated here was discretized using 161×97 grid points for the streamwise and wall-normal coordinates, respectively, and 16 Fourier modes for the spanwise direction.

3. The dynamical equations

In the following, we derive equations for the dynamical behaviour and for the energy of the coherent structures. This derivation will be based on the properties of the coherent structures as defined by the eigenfunctions of a Karhunen–Loève decomposition (or proper orthogonal decomposition, POD) of the flow. We briefly review some of the properties of the Karhunen–Loève eigenfunctions that are particularly relevant to our research; however, we do not go into details of the POD method itself. For a short basic description of the fundamental approach of this method, the reader is referred to Rempfer & Fasel (1994). A more detailed and complete account is given by Lumley (1970), Sirovich (1987), and Berkooz *et al.* (1993).

In contrast to our previous paper (Rempfer & Fasel 1994), the coherent structures for the investigations reported here were calculated from the fluctuating flow, $\boldsymbol{u}' = \boldsymbol{u} - \boldsymbol{u}_B$, where $\boldsymbol{u}_B = \langle \boldsymbol{u} \rangle$ denotes the mean flow. We use the angle brackets $\langle \cdot \rangle$ to describe time averages that, in our case of equally spaced time steps, reduce to ordinary arithmetic mean values. For convenience of notation we also use the symbol $\boldsymbol{\sigma}_0 = \langle \boldsymbol{u} \rangle$ for the base flow.

The eigenfunctions $\boldsymbol{\sigma}_i(\boldsymbol{x})$ of the POD giving the three-dimensional velocity fields of the coherent structures form an orthogonal system and we normalize them according to

$$(\boldsymbol{\sigma}_i, \boldsymbol{\sigma}_j) = \lambda_i \delta_{ij}, \tag{3.1}$$

where the parentheses $(\cdot,\cdot)$ denote the scalar product

$$(\boldsymbol{\sigma}_i, \boldsymbol{\sigma}_j) = \int_D \boldsymbol{\sigma}_i(\boldsymbol{x}) \cdot \boldsymbol{\sigma}_j(x)\, \mathrm{d}\boldsymbol{x} \tag{3.2}$$

in the Hilbert space of square-integrable, real functions (D is the three-dimensional domain considered). In (3.1), δ_{ij} denotes the Kronecker-Symbol, and λ_i are the eigenvalues of the Karhunen–Loève decomposition corresponding to the eigenfunctions $\boldsymbol{\sigma}_i$. This set of eigenfunctions is complete in the sense that the flow fields of the given ensemble can be expanded in the eigenfunctions via

$$\boldsymbol{u}^{\ell}(\boldsymbol{x}) = \boldsymbol{u}(\boldsymbol{x}, t_\ell) = \sum_i \zeta_i(t_\ell)\boldsymbol{\sigma}_i(\boldsymbol{x}), \quad i = 0, 1, 2, \ldots, \tag{3.3}$$

where

$$\zeta_0(t) \equiv 1, \quad \zeta_i(t_\ell) = \frac{(\boldsymbol{u}^{\ell}, \boldsymbol{\sigma}_i)}{\lambda_i}, \quad i > 0. \tag{3.4}$$

The expansion coefficients are uncorrelated in time and, with the normalization (3.1), their mean-square values equal unity,

$$\langle \zeta_i \zeta_j \rangle = \delta_{ij}. \tag{3.5}$$

The eigenfunctions $\boldsymbol{\sigma}_i$ can be represented as linear combinations of the instantaneous flow fields,

$$\boldsymbol{\sigma} = \sum_\ell q_\ell \boldsymbol{u}^{\ell}, \tag{3.6}$$

so that these eigenfunctions inherit all those properties of the instantaneous flow fields that can be described by linear, homogeneous time-independent equations. Thus, it is clear from (3.6) that, in our case, the eigenfunctions $\boldsymbol{\sigma}_i$ describe solenoidal vector fields representing kinematically possible velocity fields of an incompressible flow.

It has also been demonstrated (Rempfer & Fasel 1994) that the Karhunen–Loève problem for the spatially evolving boundary layer is near degenerate, yielding pairs of eigenfunctions with almost identical eigenvalues (see also Aubry, Guyonnet & Lima 1992). In Rempfer & Fasel (1994) we concluded that the dynamical coherent structures $\boldsymbol{\varsigma}_i(\boldsymbol{x}, t)$ of our transitional boundary layer are represented by pairs of eigenfunctions with almost identical eigenvalues according to

$$\boldsymbol{\varsigma}_i(x, y, z, t) = \zeta_{2i-1}(t)\boldsymbol{\sigma}_{2i-1}(x, y, z) + \zeta_{2i}(t)\boldsymbol{\sigma}_{2i}(x, y, z), \quad i = 1, 2, \ldots. \tag{3.7}$$

Each of these pairs of eigenfunctions describes a coherent structure that is moving in the streamwise direction. In parantheses we note that for the case of a parallel flow where structures of constant shape are travelling downstream at constant speed, the eigenvalue problem of the POD would be exactly degenerate, yielding pairs of identical eigenvalues, and corresponding pairs of eigenfunctions that are exact phase-shifted copies of each other. We will refer to $\boldsymbol{\varsigma}_i$ as the 'coherent structure of order i' or the 'ith-order coherent structure'.

Our goal is the derivation of a low-dimensional model of the flow in the form of a set of ordinary differential equations for the dynamical behaviour of the coherent

structures. To be able to do this, we first have to discuss the problem of boundary conditions. The boundary conditions at the wall, $y = 0$, and at the free-stream boundary, $y = y_{max}$, as well as the boundary conditions for the spanwise direction, can be expressed by linear homogeneous equations. At the wall, we simply have $\boldsymbol{u} = 0$, and for the free-stream boundary Rist & Fasel (1994) used conditions of the form

$$\frac{\partial u}{\partial y} + cu = 0, \quad c > 0, \tag{3.8}$$

corresponding to exponential decay. For the spanwise direction, periodicity was enforced by the Fourier representation chosen. From the property given in (3.6), it can be readily seen that these boundary conditions are met by each of the eigenfunctions individually.

However, we do not know *a priori* what the boundary conditions at the in- and outflow boundaries should be. As we are considering only a subregion of the integration domain of the direct simulation, the streamwise boundary conditions used in the simulation (Kloker *et al.* 1993) do not apply to our problem. It is tempting to argue that, as these boundaries are just virtual ones that do not have any physical correspondence in the real flow, they should impose no forces on the coherent structures. This argument is not valid because, in principle, influences via pressure fluctuations from upstream or downstream of the domain considered are indeed possible. In the work of Aubry *et al.* (1988), for instance, such influences had to be modelled because the flow in the subdomain of the boundary layer being treated – only the near-wall region of the flow was considered – is virtually driven by such pressure fluctuations from 'outside', which in that case are acting on the upper (free-stream) boundary. On the other hand, Deane *et al.* (1991) did not have to account for their boundary conditions separately because of either periodicity assumptions for the channel flow that they studied, or because of homogeneous conditions in their other case of a flow past a cylinder. In Noack & Eckelmann (1993), problems with the boundary conditions could be avoided by constructing a basis of eigenfunctions each of which individually satisfies each of the boundary conditions. Here, in our model we will introduce the additional *assumption* that influences from the upstream and downstream boundaries can be neglected. Then, after deriving the dynamical equations using this assumption, we will demonstrate that the simplification involved can indeed be justified.

We can start from the precondition that all of the boundary conditions are already met by each of the eigenfunctions $\boldsymbol{\sigma}_i$. As the continuity equation for incompressible flow, $\nabla \cdot \boldsymbol{\sigma}_i = 0$, is also met by each of the eigenfunctions, the dynamics of the coherent structures should be prescribed by the momentum equation of the flow alone. For the case of incompressible flow without volume forces, this equation reads

$$\frac{\partial \boldsymbol{u}}{\partial t} + \boldsymbol{u} \cdot \nabla \boldsymbol{u} = -\frac{1}{\rho} \nabla p + \nu \Delta \boldsymbol{u}, \tag{3.9}$$

where ν denotes the kinematic viscosity. Introducing the expansion (3.3) and applying a Galerkin procedure to the resulting equation is, however, not completely straightforward owing to the pressure term in (3.9). As the pressure is connected to the velocities via the Poisson equation

$$\frac{1}{\rho} \Delta p = \nabla \boldsymbol{u} : (\nabla \boldsymbol{u})^T, \tag{3.10}$$

the pressure is a nonlinear functional of the velocities, and there is no simple

representation of this term in the expansion coefficients ζ_i. We can transform the volume integral for the pressure term that results from the Galerkin procedure to a surface integral of the form

$$\int_{\partial D} p\boldsymbol{\sigma}_i \cdot \boldsymbol{n}\,\mathrm{d}S, \tag{3.11}$$

where $\boldsymbol{n}$ is the outward normal on the domain D considered. It is then readily seen that this integral will, in our case, yield contributions only for the inflow and outflow boundaries of D, and these contributions are often assumed to be small (Rajaee, Karlsson & Sirovich 1994). Our assumption concerning the influence of the boundary conditions as discussed above does exactly correspond to the omission of this pressure term.

There is, however, an alternative way to derive the evolution equations, that we present in the following. Eliminating the pressure in (3.9) by taking the curl, we get the vorticity transport equation

$$\frac{\partial \boldsymbol{\omega}}{\partial t} = \boldsymbol{\omega} \cdot \nabla \boldsymbol{u} - \boldsymbol{u} \cdot \nabla \boldsymbol{\omega} + \nu \Delta \boldsymbol{\omega}, \tag{3.12}$$

with the vorticity vector $\boldsymbol{\omega} = \nabla \times \boldsymbol{u}$. To get an evolution equation for the coherent structures, we introduce the expansion (3.3) of the flow field in the eigenfunctions of the POD. The vorticity required in (3.12) is given by

$$\boldsymbol{\omega}(x, y, z, t) = \sum_i \zeta_i(t) \boldsymbol{\sigma}_i^{\omega}(x, y, z), \tag{3.13}$$

where $\boldsymbol{\sigma}_i^{\omega}$ is the vorticity field of $\boldsymbol{\sigma}_i$,

$$\boldsymbol{\sigma}_i^{\omega} = \nabla \times \boldsymbol{\sigma}_i = \sum_{\ell} q_{\ell} \boldsymbol{\omega}^{\ell}. \tag{3.14}$$

Introducing (3.3) and (3.13) in (3.12) we arrive at

$$\sum_i \frac{\mathrm{d}\zeta_i}{\mathrm{d}t} \boldsymbol{\sigma}_i^{\omega} = \sum_{i,j} (\boldsymbol{\sigma}_i^{\omega} \cdot \nabla \boldsymbol{\sigma}_j - \boldsymbol{\sigma}_i \cdot \nabla \boldsymbol{\sigma}_j^{\omega}) \zeta_i \zeta_j + \sum_i \nu \zeta_i \Delta \boldsymbol{\sigma}_i^{\omega}. \tag{3.15}$$

By applying Galerkin projection to the equation above, claiming that the equation holds exactly within the function space spanned by the $\boldsymbol{\sigma}_i^{\omega}$, we get the system of ordinary differential equations

$$\sum_j T_{ij} \frac{\mathrm{d}\zeta_j}{\mathrm{d}t} = \sum_{j,k} \check{N}_{ijk} \zeta_j \zeta_k + \sum_j \nu \check{D}_{ij} \zeta_j, \tag{3.16}$$

where

$$T_{ij} = (\boldsymbol{\sigma}_i^{\omega}, \boldsymbol{\sigma}_j^{\omega}), \tag{3.17}$$

$$\check{N}_{ijk} = (\boldsymbol{\sigma}_i^{\omega}, \boldsymbol{\sigma}_j^{\omega} \cdot \nabla \boldsymbol{\sigma}_k - \boldsymbol{\sigma}_j \cdot \nabla \boldsymbol{\sigma}_k^{\omega}), \tag{3.18}$$

$$\check{D}_{ij} = (\boldsymbol{\sigma}_i^{\omega}, \Delta \boldsymbol{\sigma}_j^{\omega}). \tag{3.19}$$

The matrix $\boldsymbol{T}$ on the left-hand side of (3.16) is a consequence of the fact that the vorticities $\boldsymbol{\sigma}_i^{\omega}$ of the eigenfunctions $\boldsymbol{\sigma}_i$, in general, will not form an orthogonal system (but they will still form a linear independent system). Multiplying with the inverse $\boldsymbol{T}^{-1}$ we finally get

$$\frac{\mathrm{d}\zeta_i}{\mathrm{d}t} = \sum_{j,k} N_{ijk} \zeta_j \zeta_k + \nu \sum_j D_{ij} \zeta_j \tag{3.20}$$

with

$$N_{ijk} = \sum_l T_{il}^{-1} \check{N}_{ljk}, \tag{3.21}$$

$$D_{ij} = \sum_l T_{il}^{-1} \check{D}_{lj}. \tag{3.22}$$

We note that the inversion of the matrix $\boldsymbol{T}$ is, in general, not a trivial procedure within the framework of a Galerkin projection. In order to keep the truncation error under control, actually this (infinite-order) matrix would have to be inverted *before* the system is truncated, which is of course not possible. In our case, however, the matrix $\boldsymbol{T}$ is almost diagonal (or, in other words, the Karhunen–Loève eigenfunctions of the vorticity field of the flow are almost identical with the vorticities of the eigenfunctions of the velocity field). Therefore it is plausible that our course of action does not introduce large additional errors in the coefficients N_{ijk} and D_{ij}. We did check this by deriving our dynamical equations both in the primitive-variables formulation (3.9) as well as in the vorticity-transport formulation (3.12). We found that the equations derived from (3.12) were able to model the dynamics of our coherent structures more faithfully than the ones derived from(3.9)†.

Equation (3.20) describes the temporal evolution of the expansion coefficients $\zeta_i(t)$ and thus the dynamical behaviour of the coherent structures. The first, quadratic term on the right-hand side of (3.20) describes nonlinear interactions between the coherent structures, and the second term describes the influence of viscosity on the motion of the structures.

Before proceeding with the energy equations, we will show that the decision to neglect the influence of the upstream and downstream boundaries is justified. Towards this end, a comparison of the evolution in time of the expansion coefficient $\zeta_5(t)$ as calculated by integration of (3.20) to the time behaviour of this coefficient as calculated from data of the direct numerical simulation by Kloker (1993) is shown in figure 2. The dashed line was obtained by evaluating (3.4) using the data base delivered by the direct simulation. As can be seen, extremely good agreement is obtained, indicating that, indeed, in our case the influence of the boundaries can be neglected.

In deriving the energy equations of the coherent structures, we define the energy of the flow by

$$e(t) = \frac{1}{2} \int_D \boldsymbol{u}^2(\boldsymbol{x}, t)\, \mathrm{d}\boldsymbol{x}. \tag{3.23}$$

The contribution of an eigenfunction $\boldsymbol{\sigma}_i$ to the energy of the flow is given by

$$e_i(t) = \tfrac{1}{2}\lambda_i \zeta_i^2(t), \tag{3.24}$$

so that

$$\frac{\mathrm{d}e_i}{\mathrm{d}t} = \frac{\mathrm{d}(\frac{1}{2}\lambda_i \zeta_i^2)}{\mathrm{d}t} = \lambda_i \zeta_i \frac{\mathrm{d}\zeta_i}{\mathrm{d}t}. \tag{3.25}$$

Using (3.20), we arrive at

$$\frac{\mathrm{d}e_i}{\mathrm{d}t} = \lambda_i \sum_{j,k} N_{ijk} \zeta_i \zeta_j \zeta_k + \nu \lambda_i \sum_j D_{ij} \zeta_i \zeta_j. \tag{3.26}$$

† We note, however, that this difference cannot be attributed to the omission of the pressure term in the second case. By using the pressure fields as calculated in the direct simulation and adding the pressure term to the right-hand side of the model equations we could verify that the influence of this term can indeed be neglected.

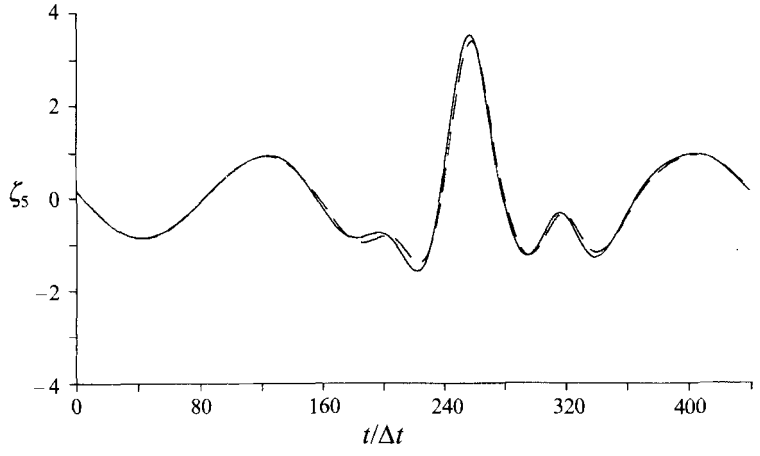

FIGURE 2. Comparison of ζ_5-coefficients as calculated from data of direct numerical simulation to the behaviour as computed by integration of (3.20): ————, model; — — —, direct simulation.

Equation (3.26) describes the variation in time of the energy of the flow field being induced by the eigenfunction with index i depending on the values of all the expansion coefficients. The first term on the right-hand side of (3.26) describes variations of the energy that are due to the nonlinear terms of the Navier–Stokes equations. The second term on the right-hand side describes the influence of dissipation on the energy of the flow field induced by the eigenfunction $\boldsymbol{\sigma}_i$.

Additional understanding can be obtained by looking at the time average of (3.26). Because the expansion coefficients are uncorrelated in time, equation (3.5), we get

$$\underbrace{\lambda_i \sum_{j,k} N_{ijk}\langle\zeta_i\zeta_j\zeta_k\rangle}_{\mathscr{P}_i} + \underbrace{\nu\lambda_i D_{ii}}_{\mathscr{D}_i} = 0. \tag{3.27}$$

This equation contains the 'production term' $\mathscr{P}_i$ and the 'dissipation term' $\mathscr{D}_i$. The elements on the main diagonal of $\boldsymbol{D}$ are all negative, so $\mathscr{D}_i$ describes the energy loss of the flow field being induced by $\boldsymbol{\sigma}_i$ that is due to dissipation. Thus, it is clear why $\mathscr{P}_i$ is called a 'production term': this term denotes the energy gain of the flow field corresponding to $\boldsymbol{\sigma}_i$ that is due to interactions with other structures and the base flow. This energy gain has to balance the continuous loss of energy caused by dissipation. $\mathscr{P}_i$ is a sum of the terms

$$\bar{\Pi}_{ijk} = \lambda_i N_{ijk}\langle\zeta_i\zeta_j\zeta_k\rangle, \tag{3.28}$$

which give the average energy gain (or loss) of the flow field being induced by $\boldsymbol{\sigma}_i$ from the interaction with the flow fields corresponding to $\boldsymbol{\sigma}_j$ and $\boldsymbol{\sigma}_k$.

Concerning these interaction terms, $\bar{\Pi}_{ijk}$, some additional remarks are in order. It should be noted that the interactions described by the instantaneous values $\Pi_{ijk}(t) = \lambda_i N_{ijk}\zeta_i(t)\zeta_j(t)\zeta_k(t)$ are, in general, non-conservative. Thus, for example, a sum of terms $\Pi_{ijk} + \Pi_{ikj} + \Pi_{jki} + \Pi_{jik} + \Pi_{kij} + \Pi_{kji}$, in general, will not be zero or, to choose a still more elementary example, terms like Π_{iii}, describing a 'self-interaction' of an eigenfunction, do not vanish in general. The reason for this is that a certain flow field formed by the superposition of certain eigenfunctions can act as an energy source

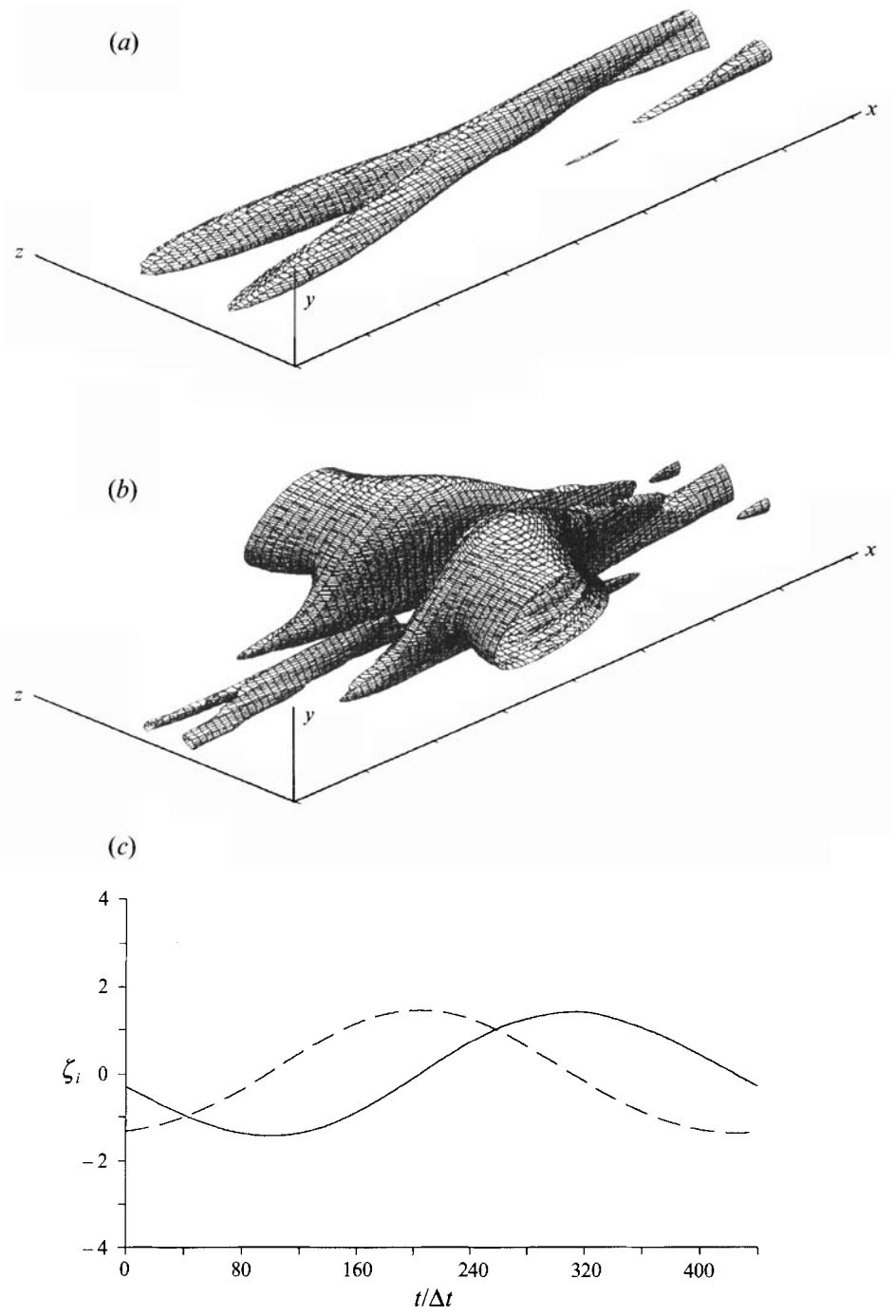

FIGURE 3. Isosurfaces and time behaviour of first-order structure, contribution to disturbance energy: 81.8%. (403 mm $\leqslant x \leqslant$ 450 mm). (*a*) Isosurface $u = 0.6\,m\,s^{-1}$. (*b*) Isosurface $v = 0.06\,m\,s^{-1}$. (*c*) Time behaviour of ζ-coefficients: ————, ζ_1; — — —, ζ_2.

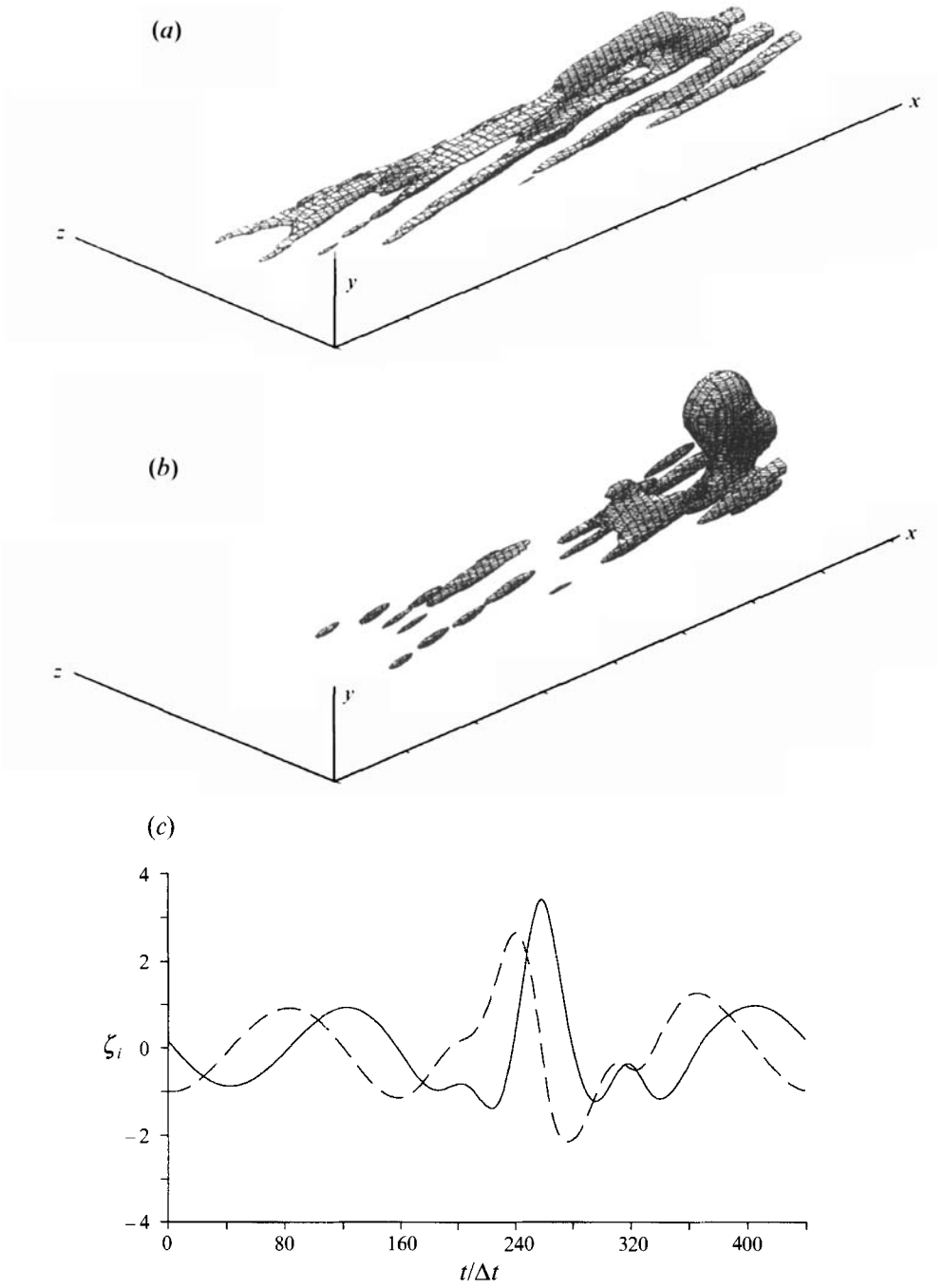

FIGURE 4. Isosurfaces and time behaviour of third-order structure, contribution to disturbance energy: 2.38%. (403 mm $\leqslant x \leqslant$ 450 mm). (*a*) Isosurface $u = 0.3\,m\,s.^{-1}$. (*b*) Isosurface $v = 0.1\,m\,s^{-1}$. (*c*) Time behaviour of ζ-coefficients: ————, ζ_5; — — —, ζ_6.

(or sink) just because of the structure of the corresponding velocity distributions. Of course, the averaged terms $\bar{\Pi}_{ijk}$ are likewise non-conservative.

Four different kinds of interactions can be discerned.

(*a*) 'Self-interactions' of the velocity field of an eigenfunction. Because $\Pi_{iii} = \lambda_i N_{iii} \zeta_i^3$, these energy flows change sign according to ζ_i.

(*b*) Binary interactions, which can be subdivided into

(i) terms of the form Π_{iji} and Π_{iij}. The sign of these terms only depends on the sign of ζ_j. Because Π_{iji} and Π_{iij} show exactly the same kind of dependency on the ζ-coefficients, they both describe the same interaction. We will therefore lump the two into one single term below.

(ii) terms of the form Π_{ijj}, the sign of which only depends on ζ_i.

(*c*) Tertiary interactions of the flow fields of three eigenfunctions. Again, the two terms Π_{ijk} and Π_{ikj} describe the same interaction and are lumped in the following.

It has been shown (Rempfer & Fasel 1994) that the dynamical coherent structures of the flow are formed by the superposition of a pair of eigenfunctions (see (3.7)). Therefore, from a coherent-structures point of view, we are more interested in the energy flows between the coherent structures than in those between eigenfunctions. Accordingly, we define the energy e_i^ς of a coherent structure by

$$e_i^\varsigma(t) = \tfrac{1}{2}(\lambda_{2i-1}\zeta_{2i-1}^2(t) + \lambda_{2i}\zeta_{2i}^2(t)), \tag{3.29}$$

and we will investigate the average production $\mathscr{P}_i^\varsigma$ of the ith-order coherent structure

$$\mathscr{P}_i^\varsigma = \lambda_{2i-1} \sum_{j,k} N_{(2i-1)jk} \langle \zeta_{2i-1}\zeta_j\zeta_k \rangle + \lambda_{2i} \sum_{j,k} N_{(2i)jk} \langle \zeta_{2i}\zeta_j\zeta_k \rangle, \tag{3.30}$$

as well as the average dissipation $\mathscr{D}_i^\varsigma$,

$$\mathscr{D}_i^\varsigma = \nu\lambda_{2i-1} D_{(2i-1)(2i-1)} + \nu\lambda_{2i} D_{(2i)(2i)}. \tag{3.31}$$

The contributions of the different interactions will also be summed over the pairs of eigenfunctions involved,

$$\check{\Pi}_{ijk}^\varsigma = \sum_{l=2i-1}^{2i} \sum_{m=\max(0,2j-1)}^{2j} \sum_{n=\max(0,2k-1)}^{2k} \Pi_{lmn}, \quad i = 1,2,\ldots,\ j,k = 0,1,\ldots. \tag{3.32}$$

Because of the above-mentioned fact that terms like $\check{\Pi}_{ijk}^\varsigma$ and $\check{\Pi}_{ikj}^\varsigma$ describe the same kind of interaction, we will finally summarize them and define the *interaction* Π_{ijk}^ς of coherent structures by

$$\Pi_{ijk}^\varsigma = \check{\Pi}_{ijk}^\varsigma + \check{\Pi}_{ikj}^\varsigma, \quad k \neq j, \qquad \Pi_{ijj}^\varsigma = \check{\Pi}_{ijj}^\varsigma. \tag{3.33}$$

The considerations given above concerning the interactions between eigenfunctions can be transferred analogously to the case of interactions between coherent structures.

4. Coherent structures of the spike stages

In the next sections, we investigate in detail the averaged and the instantaneous energy flows between the coherent structures using a set of 17 of the most energetic structures. All the results presented in the following will be based on equations derived for this set of structures that comprises 34 eigenfunctions of the Karhunen–Loève decomposition. The corresponding coefficients N_{ijk} and D_{ij} were calculated by numerically integrating the scalar products (3.21) and (3.22) using the second-order

i	$\langle e_i^\varsigma \rangle$	ε_i^ς
1	8.01×10^{-7}	8.18×10^{-1}
2	9.29×10^{-8}	9.49×10^{-2}
3	2.33×10^{-8}	2.38×10^{-2}
4	2.00×10^{-8}	2.04×10^{-2}
5	1.19×10^{-8}	1.22×10^{-2}
6	8.18×10^{-9}	8.36×10^{-3}
7	5.52×10^{-9}	5.64×10^{-3}
8	4.19×10^{-9}	4.28×10^{-3}
9	2.85×10^{-9}	2.91×10^{-3}
10	2.15×10^{-9}	2.20×10^{-3}
11	1.70×10^{-9}	1.73×10^{-3}
12	1.15×10^{-9}	1.18×10^{-3}
13	8.53×10^{-10}	8.71×10^{-4}
14	6.38×10^{-10}	6.52×10^{-4}
15	4.56×10^{-10}	4.66×10^{-4}
16	3.56×10^{-10}	3.64×10^{-4}
17	2.63×10^{-10}	2.69×10^{-4}

TABLE 1. Absolute and relative energies of the first 17 Karhunen–Loève eigenfunctions (absolute energies are given in m^5/s^2).

trapezoidal rule. Note that in order to get the terms of the energy equations discussed above, it is not necesssary to actually integrate the system (3.20). The ζ-coefficients that are needed for the evaluation of these terms are already known from the data of the direct numerical simulation via (3.4).

The relative energies of these 17 structures are given in this section to enable mental visualization. Also, certain details concerning the appearance and behaviour of two selected structures that play a particularly important role in the following treatment are presented. A more detailed account of the phenomenology of the structures at the spike stages of transition can be found in Rempfer & Fasel (1994).

The averaged absolute energies $\langle e_i^\varsigma \rangle$ are given in table 1, along with the relative energies ε_i^ς of the structures considered, where

$$\varepsilon_i^\varsigma = \frac{\langle e_i^\varsigma \rangle}{\sum_{j=1}^{440} \langle e_j^\varsigma \rangle}. \tag{4.1}$$

These relative energies give a first hint of the contribution of the structures towards the overall dynamics of the flow. It can be seen that the 17 structures considered here capture more than 99.8% of the energy of the disturbance flow $\boldsymbol{u}'$. Of these, the first-order structure alone captures almost 82% of the disturbance energy. The energies of the higher-order structures show approximately exponential decay. This is an indication of the fast convergence of the Karhunen–Loève decomposition and it can indeed be shown (Lumley 1970) that, of all possible decompositions, the one defined by the Karhunen–Loève procedure needs the smallest number of modes to represent the flow field to a given accuracy in the energy.

Figures 3 and 4 show the first- and third-order structures, the structures being represented by isosurfaces of the streamwise (u-) and the wall-normal (v-) velocity components. Additionally, in these figures, the time behaviour of the expansion

coefficients corresponding to the eigenfunctions that form the structures are shown, giving an idea of the dynamical behaviour of the structures. In the case of the first-order structure the contour surface of the u-velocity component shows the shape of the well-known Λ-vortex. This Λ-vortex is in fact the most prominent structure of the transitional boundary layer within the region we are investigating here, and has also been found in numerous experiments (see, for example, Williams, Fasel & Hama 1984, and Perry, Lim & Teh 1981). From the behaviour of the corresponding expansion coefficients, it can be seen that the energy of this first-order structure, which is approximately proportional to the sum of the squares of the expansion coefficients, is almost constant in time.

In the following, we will generally use the term 'Λ-vortex' to denote this first-order coherent structure, that is, we *define* the term 'Λ-vortex' to label the first-order coherent structure at the spike stages of transition in our flat-plate boundary layer. Owing to the similarity in appearance and behaviour of our first-order structure and the entity that has been termed 'Λ-vortex' by experimentalists, we find this identification justifiable.

The second-order structure not shown here is similar in appearance to the first-order structure, the main difference being a reduction of the streamwise scales by a factor of two. Also in analogy to the first-order structure, the second one moves with a constant velocity and its energy is (almost) constant in time.

The third-order structure in figure 4 is remarkably different from the first-order one. From the v-velocity surface, it can be seen particularly clearly that most of the energy of this structure is located near the downstream end of our domain, which is where the spike signals of transition occur. From the behaviour of the expansion coefficients, it can be seen that the energy of this structure rises steeply during a certain phase of its evolution. That this behaviour is strongly connected to the occurrence of the spike signals is demonstrated in figure 5. There, the u'-signals, that are induced by the first six coherent structures, are shown for a location where the spike signal is most pronounced. It can be seen that the third-order structure yields the largest contribution to the characteristic negative spike. It is an interesting question to ask what the underlying mechanism of the sudden rise and fall of the energy of this structure could be. This question will be addressed in §6.

Note that the third-order structure discussed here corresponds to the fourth-order structure in region D_2 in our previous paper (Rempfer & Fasel 1994). The different indices are due to the fact that the region considered here is shorter and situated more downstream than the one from our preceding paper. As there is, particularly within the region of the spike stages, a rapid streamwise growth in energy of the disturbances in our boundary layer, this difference in streamwise location leads to a different numbering of the various coherent structures, since these are ordered according to their average energy.

To conclude this section, we would like to add some remarks on the general problem of identifying coherent structures using Karhunen–Loève eigenfunctions. Basically, we think that the defining properties of the POD eigenfunctions of the velocity field – in particular their energy optimality – are significant enough to warrant a detailed investigation of the entities described by these functions. Whether or not one wants to call these objects 'coherent structures' may be a matter of taste, but our previous paper shows that there indeed seems to be a close relation between the decomposition of the flow field as prescribed by the Karhunen–Loève procedure and the decomposition human observers typically perform based on their intuition. In particular, this means that there are qualitative differences in shape and/or evolution between the different

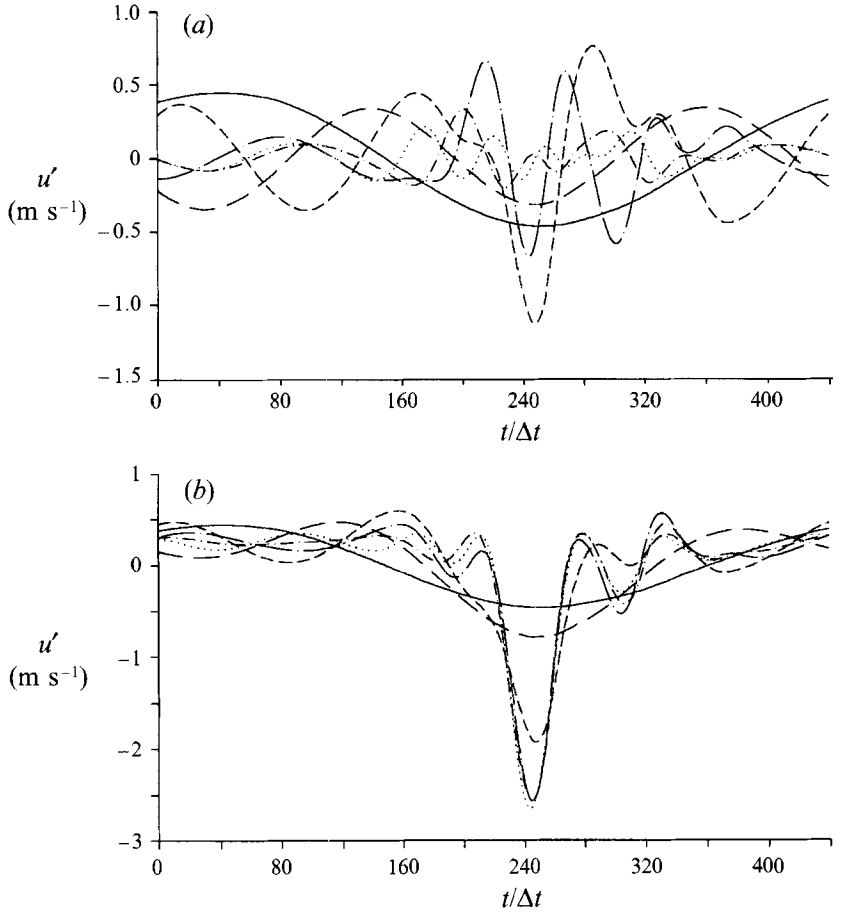

FIGURE 5. Time signals of u'-component of coherent structures at $x = 445$ mm, $y = 4.22$ mm, $z = 0$. (*a*) Time signals ————, ς_1; — — —, ς_2; – – – – – –, ς_3; ——·——, ς_4; —·—·—·—, ς_5; ·····, ς_6. (*b*) Summed time signals ————, ς_1; — — —, to ς_2; – – – – – –, to ς_3; ——·——, to ς_4; —·—·—·—, to ς_5; ·····, to ς_6.

coherent structures as defined by (3.7). For instance, the first- and third-order structures described above are completely different in their appearance as well as in their behaviour. While the first-order structure is smoothly moving downstream at almost constant energy, the third-order structure, representing an ejection-like event during a spike, is moving mainly in the wall-normal direction while hardly changing its location along the streamwise coordinate, and it shows sharp variations in its energy (see also Rempfer & Fasel 1994 for a more detailed description of the kinematics of these coherent structures). Our investigations presented here also show that certain clear-cut events of our transitional boundary layer – like the spikes – are quite well captured by the action of distinct structures ς_i, and in that sense the ς_i form a basis of physically significant eigenfunctions.

5. Average energy flows

We have investigated in detail the different contributions of the coherent structures to the averaged energy balance. Toward this end, we calculated the first 34 eigenfunc-

	$T_0\mathscr{P}_i^{\varsigma+}$		$T_0\mathscr{P}_i^{\varsigma-}$		$T_0\mathscr{D}_i^{\varsigma}$	
i	absolute	relative	absolute	relative	absolute	relative
1	1.57×10^{-6}	3.92	-2.89×10^{-7}	−0.72	-1.13×10^{-6}	−2.81
2	3.01×10^{-7}	6.48	-4.48×10^{-8}	−0.97	-2.14×10^{-7}	−4.61
3	1.23×10^{-7}	10.54	-2.61×10^{-8}	−2.24	-7.80×10^{-8}	−6.68
4	1.17×10^{-7}	11.72	-3.09×10^{-8}	−3.10	-6.81×10^{-8}	−6.84
5	7.53×10^{-8}	12.62	-1.91×10^{-8}	−3.22	-4.57×10^{-8}	−7.65
6	5.61×10^{-8}	13.70	-1.67×10^{-8}	−4.08	-3.12×10^{-8}	−7.62
7	4.09×10^{-8}	14.81	-1.39×10^{-8}	−5.03	-2.05×10^{-8}	−7.41
8	3.20×10^{-8}	15.30	-8.10×10^{-9}	−3.88	-1.79×10^{-8}	−8.55
9	2.64×10^{-8}	18.51	-7.54×10^{-9}	−5.29	-1.40×10^{-8}	−9.85
10	2.34×10^{-8}	21.77	-8.04×10^{-9}	−7.47	-1.18×10^{-8}	−10.94
11	1.81×10^{-8}	21.33	-5.83×10^{-9}	−6.86	-8.67×10^{-9}	−10.21
12	1.40×10^{-8}	24.26	-4.04×10^{-9}	−7.02	-6.21×10^{-9}	−10.78
13	1.13×10^{-8}	26.42	-2.26×10^{-9}	−5.29	-4.98×10^{-9}	−11.68
14	9.81×10^{-9}	30.75	-1.82×10^{-9}	−5.70	-4.24×10^{-9}	−13.28
15	8.46×10^{-9}	37.07	-1.23×10^{-9}	−5.38	-3.67×10^{-9}	−16.09
16	6.40×10^{-9}	36.00	-5.50×10^{-10}	−3.09	-2.81×10^{-9}	−15.82
17	5.22×10^{-9}	39.77	-6.40×10^{-10}	−4.87	-2.04×10^{-9}	−15.52

TABLE 2. Average energy gains $\mathscr{P}_i^{\varsigma+}$, losses $\mathscr{P}_i^{\varsigma-}$, and dissipation $\mathscr{D}_i^{\varsigma}$ (absolute energies are given in $\mathrm{m}^5\ \mathrm{s}^{-2}$).

tions of the Karhunen–Loève decomposition corresponding to 17 coherent structures, as well as the corresponding expansion coefficients ζ_i. We then computed the matrices N_{ijk} and D_{ij} from (3.21) and (3.22). Based on the expansion coefficients ζ_i, we were then able to determine the interactions $\bar{\Pi}_{ijk}^{\varsigma}$.

A first overview of the energy balance of the different coherent structures can be obtained from table 2, which summarizes the gains and the losses of energy for the coherent structures considered. The term $\mathscr{P}_i^{\varsigma}$ was split into the sum $\mathscr{P}_i^{\varsigma+}$ of energy gains and the sum $\mathscr{P}_i^{\varsigma-}$ of energy losses from the nonlinear interactions. The respective values were then multiplied by the integration time T_0 of the direct numerical simulation and therefore directly represent the energies that the coherent structures lost or gained in interactions or that they dissipated during that time. In a second column, these energies have been divided by the average energies of the corresponding coherent structures in order to obtain relative energy gains and losses. From the relative energies in table 2, it can be seen that the coherent structures are highly active dynamical objects. During the time T_0 – which in the case of the first-order structure is equal to the time the structure needs to move by a distance of the length of the structure itself – almost four times the energy contained in the velocity field of the structure is turned over. This behaviour is even more pronounced for the higher-order structures, which dissipate up to sixteen times their own energy.

Furthermore, it can be seen that in the case of the first-order structure, the dissipated energy almost equals the energy gain $\mathscr{P}^{\varsigma+}$ for nonlinear interactions. In other words, almost all the energy this structure obtains from the interaction with other structures is dissipated immediately. For the higher-order structures, the quotient of dissipated energy and nonlinear energy gain decreases to just below 50%; nevertheless, dissipation still represents by far the largest single contribution to the energy balance.

If gains and losses from interactions and dissipated energy are added, a surplus

	$\bar{\Pi}^{\varsigma}_{ijk}/\mathscr{P}^{\varsigma+}_{i}$					
i	j-k	%	j-k	%	j-k	%
1	0-1:	84.00	1-2:	15.54	1-1:	0.26
2	0-2:	65.17	1-1:	24.15	1-4:	3.88
3	1-2:	50.88	1-3:	16.52	0-3:	15.80
4	1-4:	33.47	1-2:	15.42	1-5:	13.18
5	1-5:	20.24	1-3:	18.77	1-6:	13.08
6	1-7:	16.25	1-4:	14.97	1-5:	13.85
7	1-8:	13.89	3-4:	11.71	1-7:	11.06
8	1-6:	15.07	1-8:	7.90	3-4:	7.70
9	1-8:	25.34	1-6:	8.32	1-7:	8.15
10	1-9:	29.30	1-5:	7.73	3-3:	6.24
11	1-10:	21.08	4-5:	8.62	4-7:	4.90
12	1-11:	19.10	4-6:	5.89	6-7:	5.87
13	4-7:	13.71	1-12:	8.15	1-11:	6.79
14	4-8:	11.98	1-12:	8.63	1-13:	6.88
15	1-14:	11.59	4-10:	5.80	7-9:	5.63
16	1-15:	13.71	4-12:	6.97	4-11:	6.68
17	1-16:	13.73	6-11:	5.95	2-13:	4.37
	$\bar{\Pi}^{\varsigma}_{ijk}/\mathscr{P}^{\varsigma-}_{i}$					
i	j-k	%	j-k	%	j-k	%
1	2-3:	33.64	2-4:	9.87	4-4:	7.75
2	2-5:	12.91	2-6:	10.58	3-4:	5.31
3	1-5:	33.97	2-4:	11.81	4-8:	6.85
4	1-6:	15.57	4-8:	9.13	3-7:	7.88
5	1-10:	6.58	1-8:	6.28	3-7:	5.12
6	2-7:	9.59	1-9:	9.36	1-8:	5.18
7	0-7:	17.08	4-13:	9.34	2-8:	6.71
8	4-14:	10.90	3-13:	9.82	0-8:	8.40
9	1-10:	27.21	0-9:	22.20	7-15:	3.64
10	0-10:	25.29	1-8:	18.99	1-11:	13.52
11	0-11:	34.80	1-13:	11.02	4-15:	6.64
12	0-12:	33.61	1-14:	15.06	4-16:	7.08
13	0-13:	43.74	2-17:	7.09	5-16:	7.04
14	0-14:	55.16	1-15:	12.20	5-17:	7.33
15	0-15:	34.90	1-16:	25.18	4-17:	7.80
16	1-17:	21.51	2-17:	12.23	3-15:	9.79
17	0-17:	65.97	4-9:	8.11	6-10:	4.02

TABLE 3. Largest gains and losses from interactions.

of energy is found that, relative to the energy turned over, increases for the higher-order structures. This phenomenon is a consequence of the fact that only a limited number of structures could be considered. Therefore, particularly for the higher-order structures, interactions with the neglected structures are missing in the energy balance.

We now address in detail the question of which interactions are the ones that deliver the energy being dissipated. Table 3 displays the largest three contributions, $\bar{\Pi}^{\varsigma}_{ijk}$, to the positive and negative production $\mathscr{P}^{\varsigma+}$ and $\mathscr{P}^{\varsigma-}$, respectively. The numbers in table 3 show the portion that the corresponding individual interaction contributes to the total gains and losses from interactions (see table 2).

Looking first at the energy gains, we can see that the first two structures get the main part of their energy from an interaction with the base flow σ_0, and an additional considerable part comes from their mutual interaction. Almost all other structures, however, get the largest positive contribution from interactions in which the first-order structure is at least partially involved. For the third-order structure, it is the interaction with the first- and second-order structures that delivers more than 50% of the dissipated energy and, for the fourth- and fifth-order structures, it is a binary interaction with the Λ-vortex that results in the largest contribution. For most of the remaining structures, the interaction with the Λ-vortex and a neighbouring structure is the most important one. Only the thirteenth and fourteenth structures are exceptional, but even there the interaction with the Λ-vortex is second in importance. Furthermore, it can be seen from the decay of the percentages that the number of interactions that substantially contribute to the energy balance of a structure is rising with the order of the structure. Thus, with rising order, the relation of the structures to other structures becomes more complex.

In contrast to the case just discussed, the situation is not as simple when considering the energy losses, at least for the first nine structures, for which we find a variety of interactions that contribute most to the losses. However, from the tenth structure on, we see that the largest loss of energy results from an interaction with the base flow. Also, the situation is just the opposite of that for the energy gains: the higher the order of a structure, the higher the portion of the interaction with the base flow.

Generally, the observations discussed above demonstrate the leading role that the Λ-vortex plays in the dynamics of the flat-plate boundary layer, in particular in the region where the spike stages occur. In view of the considerable share that the interaction with this structure contributes to the energy balance of all further structures, we can indeed conclude that all higher-order structures, and thus the dynamics of the flow as a whole, do depend strongly on the Λ-vortex. This Λ-vortex, on the other hand, gets almost all of its energy from the base flow. Changing the base flow in such a way as to stop this energy transfer would remove the preconditions for the existence of the Λ-vortex and all further structures, thus preventing transition to turbulence. However, it is quite probable that the changed base flow would then support different structures that, instead, would lead to transition. Nevertheless, it would be of interest to explore the effects of a modification of boundary conditions that would hinder the motion of the Λ-vortex.

Also, we would like to point out that the picture of an energy cascade known from the theory of homogeneous turbulence is not suitable for describing the energy flows in the system of coherent structures during transition that we are considering here. Obviously, we do not have a situation where low-order structures pass energy to higher-order ones, which in turn pass their energy to still higher-order structures. Instead, most of the structures receive their energy 'in parallel' from the base flow and the Λ-vortex. Also, energy is not mainly just passed on from structure to structure with dissipation only occurring at the very highest orders, but rather, all of the structures immediately dissipate most of the energy they receive from nonlinear interactions.

In the discussion above, we considered individual interactions between coherent structures. Now, we conclude this section with an overview of the structure of these interactions in a global sense. In other words, we are seeking answers to the question of whether the coherent structures do interact in an arbitrary fashion or whether definite schemes can be identified that exclude certain structures from interacting with other structures. To address this issue, the matrices of the averaged energy

flows, $\bar{\Pi}^{\varsigma}_{ijk}$, for some selected structures are shown in figures 6 and 7 in the form of histograms in perspective representation. In figure 6, the histograms are viewed from above so that the positive $\bar{\Pi}^{\varsigma}_{ijk}$ can be discerned most clearly. In figure 7, a view from below shows the structure of the negative contributions.

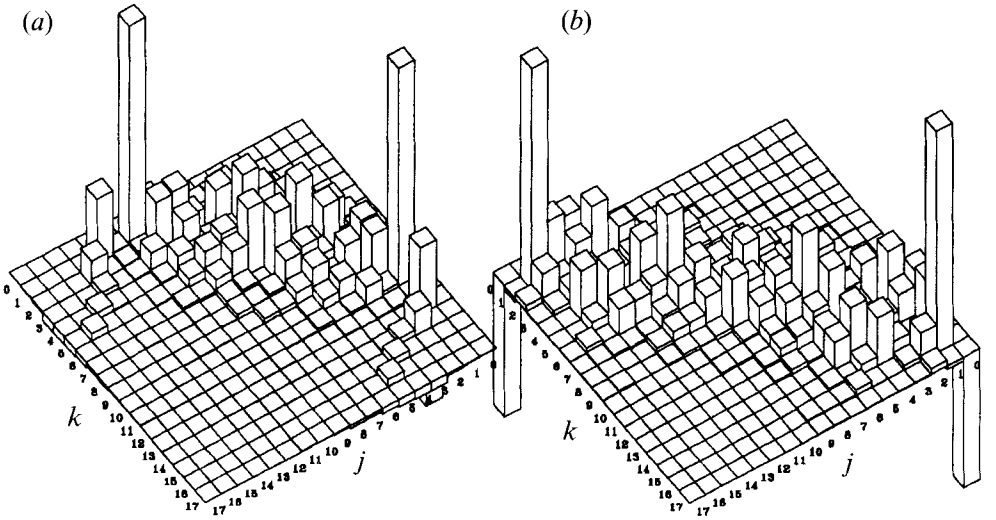

FIGURE 6. Histograms of averaged energy flows $\bar{\Pi}^{\varsigma}_{ijk}$. (*a*) 12th-order structure ($i = 12$). (*b*) 17th-order structure ($i = 17$).

It can be seen clearly that the coherent structures by no means interact arbitrarily. For the positive interactions, the significant contributions group along a diagonal described by the equation

$$i \approx j + k \tag{5.1}$$

for the indices of the structures involved, and the negative contributions occur near diagonals described by

$$i \approx |j - k|. \tag{5.2}$$

For the case of homogeneous turbulence, it can be shown (McComb 1990) that only modes, the wave vectors $\boldsymbol{i}$, $\boldsymbol{j}$, $\boldsymbol{k}$ of which form a *triad* such that $\boldsymbol{i} + \boldsymbol{j} + \boldsymbol{k} = \boldsymbol{0}$, interact. Similarly as for homogeneous turbulence, for the case of the coherent structures considered here, certain interactions described by the equations above are preferred. However, in contrast to the equations for pure spectral modes, the equations (5.1) and (5.2) are not exact, rather they are just describing a preferred pattern for the interactions. Also note that there is a basic difference between the equations for wave interactions in homogeneous turbulence and our equations (5.1) and (5.2). While the former involve *wavenumbers*, the latter describe relations between *indexing variables*. The similarity between these equations does, however, suggest a connection between the two concepts. In our case, the link lies in the fact that, for *most* of our modes, the spatial scales involved are indeed closely connected to their indices in that the most energetic spatial scales of the eigenfunctions vary inversely proportionally to the value of their index. For example, the most energetic spatial scales of the eigenfunctions forming the second-order structure are about half the size of those for the first-order structure.

Equation (5.2) for the preferred interactions for energy losses elucidates why,

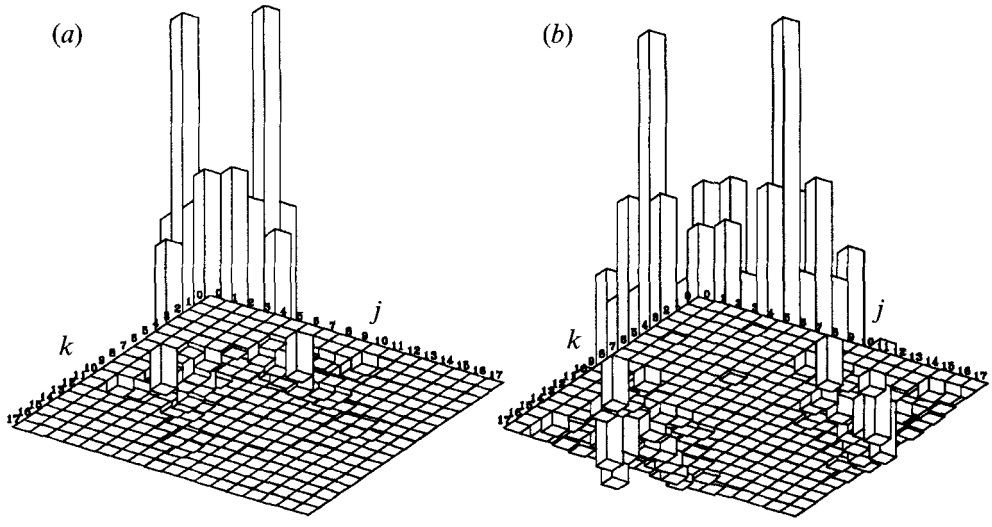

FIGURE 7. Histograms of averaged energy flows $\bar{\Pi}^{c}_{ijk}$. (*a*) 4th-order structure ($i = 4$). (*b*) 8th-order structure ($i = 8$).

especially for the higher-order structures, a surplus of energy was found in the energy balance given in table 2. In order for the above equation to hold, at least one of the indices j or k has to be larger than the index i. In other words, significant energy losses occur only in interactions with higher-order structures. By truncating the expansion of the flow field at a certain index, the highest-order structures cannot pass on their energy and thus a surplus of energy must occur in the balance.

6. Instantaneous energy flows

After the discussion of the averaged energy flows in the system of coherent structures, we will now explore the instantaneous values of the Π^{c}_{ijk} using a selected example. Looking at the time behaviour of the expansion coefficients corresponding to the third-order structure (see figure 4), a significant rise in energy of this structure can be observed between time steps 200 and 300. It was shown in §4 that this behaviour is connected to the occurrence of the characteristic spikes of the transition stage that we are investigating here. Therefore, it is of particular interest to find the causes of the strong variation in energy of the third-order structure. This variation can only be caused by nonlinear interactions.

In figure 8, the development of the energy, $e^{c}_{i}(t)$, of the first six coherent structures is shown. The most noticeable behaviour is displayed by the energy of the third-order structure. From time step 200 to 260, this energy rises to six times its mean value and more than ten times its average value from the time before. Then, to time step 320, the energy falls back again to its previous value. Thus the question arises, 'What causes these extreme variations in energy?' To explore this issue, the instantaneous values of the matrix $\Pi^{c}_{3jk}(t)$ at time step 250 (at the moment of steepest rise in energy) and at time step 270 (at the moment of steepest decay) are shown in perspective representation in figure 9.

These histograms demonstrate that, in essence, one single interaction determines the behaviour of the energy of the third-order structure. The increase as well as the

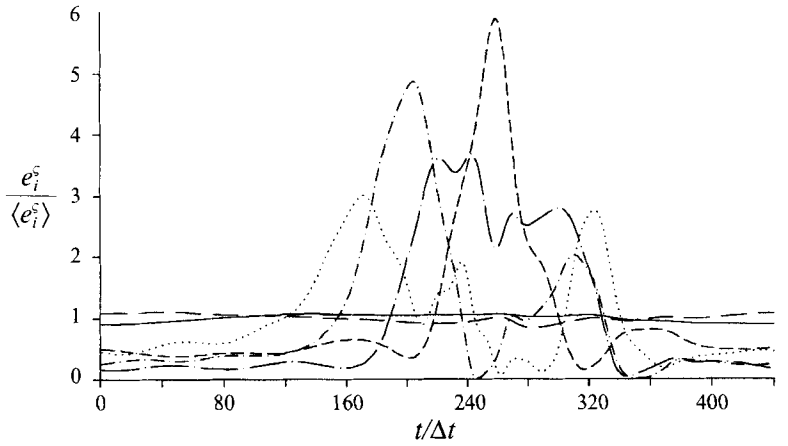

FIGURE 8. Behaviour of energy $e_i^\varsigma(t)$ of the first six structures. The energies have been divided by their time average. ————, e_1^ς; — — —, e_2^ς; – – – – –, e_3^ς; ——·——, e_4^ς; —·—·—·—, e_5^ς; ·····, e_6^ς.

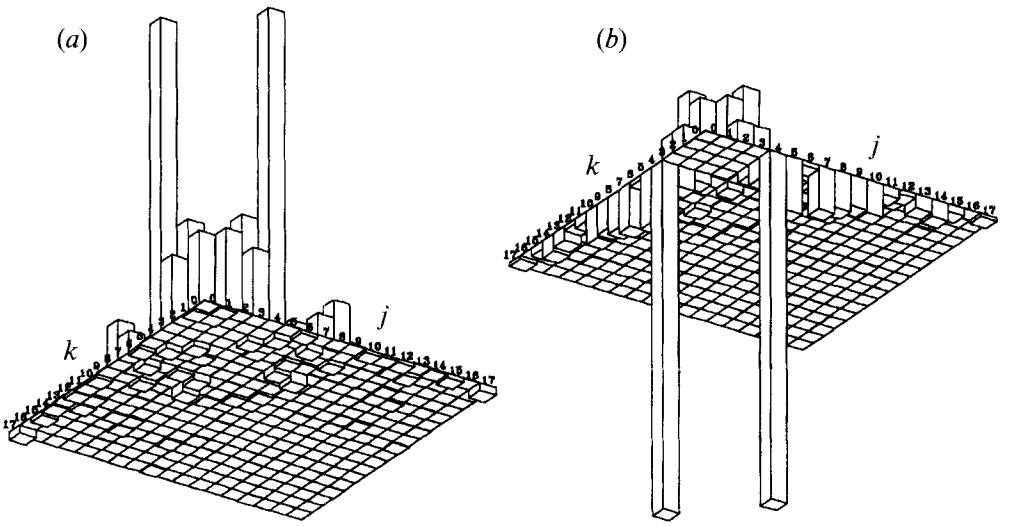

FIGURE 9. Histograms of instantaneous energy flows Π_{3jk}^ς of third-order structure ($i = 3$). (*a*) Time step $t/\Delta t = 250$. (*b*) Time step $t/\Delta t = 270$.

decrease of the energy are caused by the energy gain and loss that the third-order structure suffers in an interaction with the base flow and the fourth-order structure. This can be seen most clearly when the time derivative of the energy of the third-order structure is compared to the contributions provided by the interaction 3-0-4 (i.e. the interaction between third-order structure, base flow, and fourth-order structure) and dissipation (figure 10).

From figure 11, which shows instantaneous energy flows of the fourth-order structure in an analogous way to figure 9 (both figures are drawn using the same scale factors), one can observe a kind of alternating play: almost exactly the energy that the third-order structure gains in the interaction 3-0-4 is lost by the fourth-order structure in the interaction 4-0-3, and *vice versa*. The fact that the development of

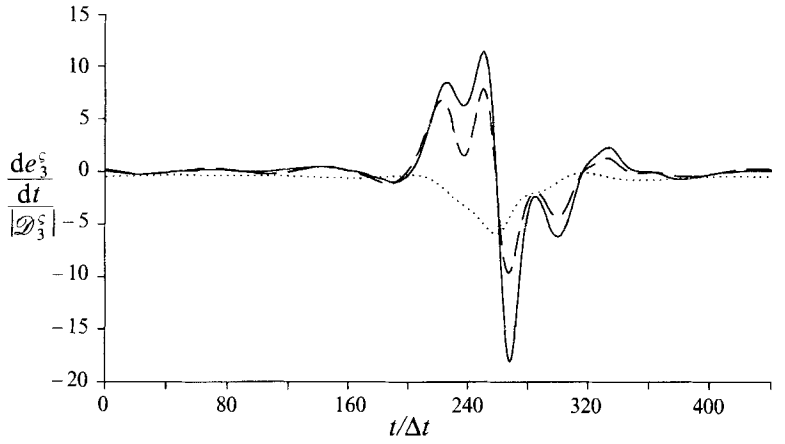

FIGURE 10. Contributions to the derivative de_3^ς/dt of the energy of the third-order structure. Values have been divided by the absolute of the average dissipation $\mathscr{D}_3^\varsigma$. ————, de_3^ς/dt; — — —, Π_{304}^ς; ·····, instantaneous dissipation.

the energy of the fourth-order structure is not just a mirror image of the one of the third-order structure is due to additional interactions which contribute to the energy balance of the fourth-order structure, as seen in figure 12.

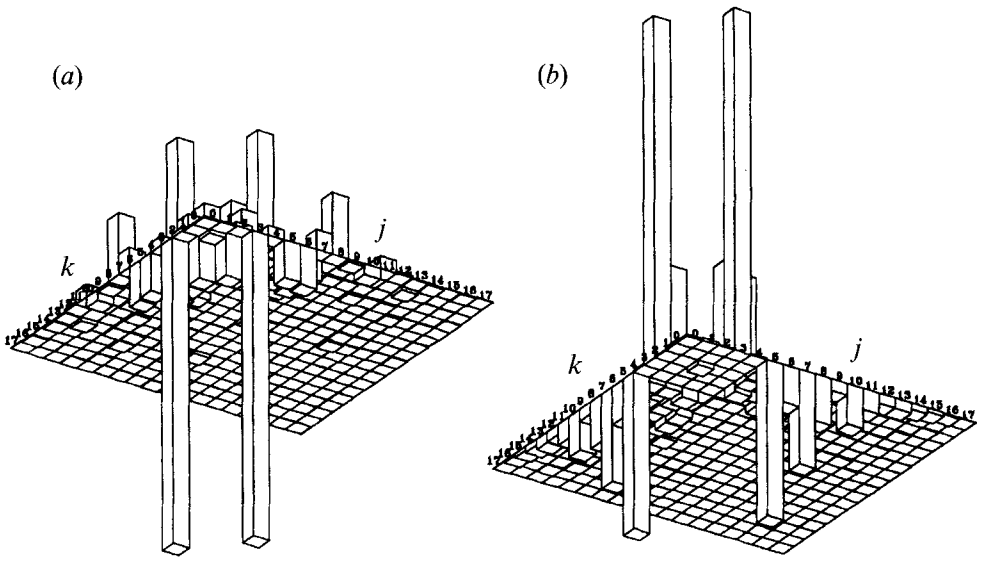

FIGURE 11. Histograms of instantaneous energy flows Π_{4jk}^ς of fourth-order structure ($i = 4$). (*a*) Time step $t/\Delta t = 250$. (*b*) Time step $t/\Delta t = 270$.

From a coherent structures point of view, the cause of spikes can thus be explained as follows. First, it should be noted that the motion of the Λ-vortex (first-order structure) alone induces some negative u' disturbance velocity (see figure 5). The sharp spike, however, is caused by a separate event. At the time instant of the formation of a spike, a certain coherent structure is 'created', the velocity field of which strongly enforces the negative deflection of the u'-signal. Although this third-

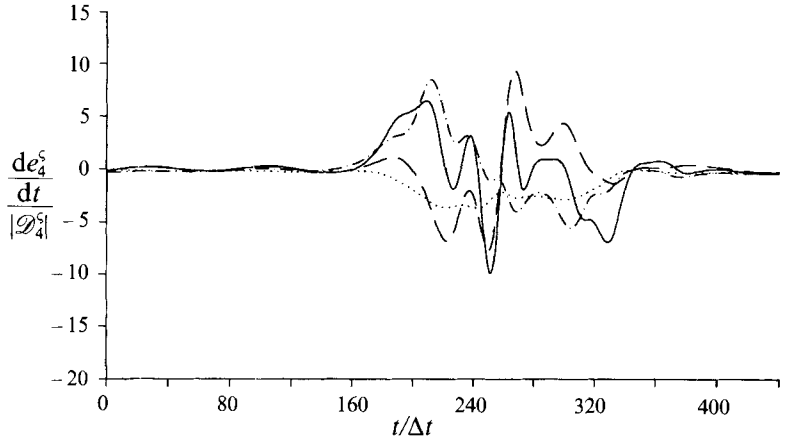

FIGURE 12. Contributions to the derivative de_4^ς/dt of the energy of the fourth-order structure. Values have been divided by the absolute of the average dissipation $\mathscr{D}_4^\varsigma$. ————, de_4^ς/dt; — — —, Π_{403}^ς; – · – · –, Π_{405}^ς; ·····, instantaneous dissipation.

order structure is actually present all the time, the term 'created' seems to be justified in view of the considerable growth of energy of this structure during the spike.

The course of events just described is completely independent of the A-vortex in the sense that the energy for the sudden growth of the third-order structure is almost completely obtained from an interaction with the base flow and the fourth-order structure and that this energy is also lost in the same interaction. On the other hand, the third-order structure is dissipating energy all the time. This dissipated energy cannot be supplied by the interaction 3-0-4 because the time average of the energy from this interaction contains only terms of the form $\lambda_i N_{ijk}\langle\zeta_i\zeta_j\rangle$ that are zero because of (3.5). The investigations of the previous section have shown that the third-order structure gets the largest part of its energy *in the time average* from an interaction with the first- and second-order structures. Thus, the A-vortex so to speak 'pays for the third-order structure's keep', but the actual spike is produced in an autonomous process where the flow fields of the third- and fourth-order structures and the base flow are superimposed in such a way that the energy of the third-order structure can rise considerably.

These considerations support our statement made on a purely phenomenological basis (Rempfer & Fasel 1994), namely, that the behaviour of the coherent structure causing the spikes indeed seems to be due to an independent process and the spike itself cannot be described as just an epiphenomenon of the passage of a A-vortex.

7. Discussion

In summary, we would like to point out the considerable advantages of the application of the POD method in connection with Galerkin projection of the Navier–Stokes equations onto the basis of Karhunen–Loève eigenfunctions. First of all, the POD method supplies a completely unambiguous, precise mathematical definition of what is meant by the term 'coherent structure'. Apart from the purely mathematical attractiveness of this definition, from our point of view, this property is one of the prime preconditions for such a notion to be meaningful. Only a strict definition actually allows comparison of results obtained by different researchers and in different

laboratories. In contrast, such strict definitions are often lacking in the conditional-sampling community, thus making it difficult to formulate statements that go beyond purely qualitative descriptions.

Furthermore, we feel that the concept of a coherent structure is of little use as long as it is not possible to give a precise and comprehensive description of the role that these structures play in the dynamics of a flow. Often, such descriptions have been limited at most to statements with regard to the contribution of a structure to the turbulent energy or an estimation of its addition to turbulent production. In contrast, by investigating the energy equation of the coherent structures in this paper, we have shown how a detailed description of the dynamics of coherent structures can be obtained. With this approach, it is possible to uncover the mechanisms behind the behaviour of the coherent structures and thus find out, so to speak, 'how the flow works'.

Certain analogies between the spikes of transitional boundary layers and the bursting event in fully turbulent boundary layers had already been suggested (Rempfer & Fasel 1994). If these analogies rest on a physical basis, then the investigations reported here should also shed some light on the phenomena occurring in turbulent boundary layers. Thus, for example, of the models for bursting in fully developed turbulent boundary layers reported by Robinson (1991), our findings would exclude all those that do not include special autonomous processes causing the actual ejection. Numerical simulations employing increased spatial and temporal resolution – which we are planning in the near future – should lead to a fully turbulent state of the boundary layer. With data from such a simulation, we will not only be able to study the bursting phenomenon directly, but we can also attempt direct and detailed comparisons between the phenomena in fully turbulent and in transitional boundary layers. Thus the fairly speculative discussion of this topic can then be placed on a quantitative basis.

Finally, by studying the system of ODE's (3.20) describing the evolution in time of the coherent structures, it is also possible to apply the well-developed methods of dynamical systems theory to the dynamics of fluid flow. Such investigations have been reported by Aubry *et al.* (1988), Deane *et al.* (1991), and Zhou & Sirovich (1992), and it is hoped that this kind of research will enhance our fundamental understanding of turbulent flows. From such studies, we may expect an answer to the question, 'What relevance do the ideas around deterministic chaos have in the case of turbulent flows?' For our flat-plate boundary layer, we have started investigations in that direction (Rempfer 1991, 1993, 1994), and this research will be extended in the future.

This research was supported by grants from the Studienstiftung des deutschen Volkes, Germany, and the Office of Naval Research, USA.

REFERENCES

AUBRY, N., GUYONNET, R. & LIMA, R. 1992 Spatio-temporal symmetries and bifurcations via bi-orthogonal decompositions. *J. Nonlin. Sci.* **2**, 683–739.

AUBRY, N., HOLMES, P., LUMLEY, J. L. & STONE, E. 1988 The dynamics of coherent structures in the wall region of a turbulent boundary layer. *J. Fluid Mech.* **192**, 115–173.

BERKOOZ, G., HOLMES, P. & LUMLEY, J. L. 1993 The proper orthogonal decomposition in the analysis of turbulent flows. *Ann. Rev. Fluid Mech.* **25**, 539–575.

BLACKWELDER, R. F. 1983 Analogies between transitional and turbulent boundary layers. *Phys. Fluids* A **26**, 2807–2815.

BROWN, G. L. & ROSHKO, A. 1974 On density effects and large structure in turbulent mixing layers. *J. Fluid Mech.* **64**, 775–816.

CANTWELL, B. J. 1981 Organized motion in turbulent flow. *Ann. Rev. Fluid Mech.* **13**, 457–515.

DEANE, A. E., KEVREKIDIS, I. G., KARNIADAKIS, G. E. & ORSZAG, S. A. 1991 Low-dimensional models for complex geometry flows: Application to grooved channels and circular cylinders. *Phys. Fluids* A **3**, 2337–2354.

EINSTEIN, H. A. & LI, H. 1956 The viscous sublayer along a smooth boundary. *J. Engng Mech. Div. ASCE* **82**(EM2): Paper 945.

FIEDLER, H. E. 1987 Coherent structures. In *Advances in Turbulence* (ed. G. Comte-Bellot & J. Mathieu), pp. 320–336. Springer.

GUPTA, A. K., LAUFER, J. & KAPLAN, R. E. 1971 Spatial structure in the viscous sublayer. *J. Fluid Mech.* **50**, 493–512.

HUSSAIN, A. K. M. F. 1983 Coherent structures – reality and myth. *Phys. Fluids* A **26**, 2816–2850.

HUSSAIN, A. K. M. F. 1986 Coherent structures and turbulence. *J. Fluid Mech.* **173**, 303–356.

KACHANOV, Y. S., KOZLOV, V. V., LEVCHENKO, V. Y. & RAMAZANOV, M. P. 1985 On nature of k-breakdown of a laminar boundary-layer. New experimental data. In *Laminar-Turbulent Transition* (ed. V. V. Kozlov), pp. 61–73. Springer.

KIM, H. T., KLINE, S. J. & REYNOLDS, W. C. 1971 The production of turbulence near a smooth wall in a turbulent boundary layer. *J. Fluid Mech.* **50**, 133–160.

KLINE, S. J., REYNOLDS, W. C., SCHRAUB, F. A. & RUNSTADLER, P. W. 1967 The structure of turbulent boundary layers. *J. Fluid Mech.* **30**, 741–773.

KLINE, S. J. & RUNSTADLER, P. W. 1959 Some preliminary results of visual studies of the flow model of the wall layers of the turbulent boundary layer. *Trans. ASME*, E: *J. Appl. Mech.* **2**, 166–170.

KLOKER, M. 1993 Direkte numerische Simulation des laminar-turbulenten Strömungsumschlages in einer stark verzögerten Grenzschicht. Dissertation, University of Stuttgart.

KLOKER, M., KONZELMANN, U. & FASEL, H. 1993 Outflow boundary conditions for spatial Navier-Stokes simulations of transition boundary layers. *AIAA J.* **31**, 620–628.

LOÈVE, M. 1955 *Probability theory*. Van Nostrand.

LUMLEY, J. L. 1967 The structure of inhomogeneous turbulent flows. In *Atmospheric Turbulence and Radio Wave Propagation* (ed. A. M. Yaglom & V. I. Tatarski), pp. 166–178. Nauka, Moscow.

LUMLEY, J. L. 1970 *Stochastic Tools in Turbulence*. Academic.

MCCOMB, W. D. 1990 *The Physics of Fluid Turbulence*. Clarendon.

MONIN, A, S. & YAGLOM, A. M. 1973 *Statistical Fluid Mechanics*. MIT Press.

NOACK, B. R. & ECKELMANN, H. 1993 A low-dimensional Galerkin method for the three-dimensional flow around a circular cylinder. *Phys. Fluids* A **6**, 124–143.

PERRY, A. E., LIM, T. T. & TEH, E. W. 1981 A visual study of turbulent spots. *J. Fluid Mech.* **104**, 387–405.

RAJAEE, M., KARLSSON, S. K. F. & SIROVICH, L. 1994 Low-dimensional description of free-shear-flow coherent structures and their dynamical behaviour. *J. Fluid Mech.* **258**, 1–29.

REMPFER, D. 1991 Kohärente Strukturen und Chaos beim laminar-turbulenten Grenzschichtumschlag. Dissertation, University of Stuttgart.

REMPFER, D. 1993 Low-dimensional models of a flat-plate boundary layer. In *Near-Wall Turbulent Flows* (ed. R. M. C. So, C. G. Speziale & B. E. Launder), pp. 63–72. Elsevier.

REMPFER, D. 1994 On the structure of dynamical systems describing the evolution of coherent structures in a convective boundary layer. *Phys. Fluids* **6**, 1402–1404.

REMPFER, D. & FASEL, H. 1994 Evolution of three-dimensional coherent structures in a flat-plate boundary layer. *J. Fluid Mech.* **260**, 351–375.

REYNOLDS, O. 1883 On the experimental investigation of the circumstances which determine whether the motion of water shall be direct or sinuous, and the law of resistance in parallel channels. *Phil. Trans. R. Soc. Lond.* **174**, 935–982.

RIST, U. & FASEL, H. 1994 Direct numerical simulation of controlled transition in a flat-plate boundary layer. (to appear in *J. Fluid Mech.*)

ROBINSON, S. K. 1991 Coherent motions in the turbulent boundary layer. *Ann. Rev. Fluid Mech.* **23**, 601–639.

RUNSTADLER, P. G., KLINE, S. J. & REYNOLDS, W. C. 1963 An experimental investigation of flow struc-

ture of the turbulent boundary layer. *Rep.No.* MD-8 Dept Mech. Engng, Stanford University Stanford, CA.

SIROVICH, L. 1987 Turbulence and the dynamics of coherent structures. *Q. Appl. Maths* **45**, 561–590.

TOWNSEND, A. A. 1956 *The Structure of Turbulent Shear Flow.* Cambridge University Press.

WALLACE, J. M., ECKELMANN, H. & BRODKEY, R. S. 1972 The wall region in turbulent shear flow. *J. Fluid Mech.* **54**, 39–48.

WILLIAMS, D. R., FASEL, H. & HAMA, F. R. 1984 Experimental determination of the three-dimensional vorticity field in the boundary-layer transition process. *J. Fluid Mech.* **149**, 179–203.

WILLMARTH, W. W. & LU, S. S. 1972 Structure of the Reynolds stress near the wall. *J. Fluid Mech.* **55**, 65–92.

ZHOU, X. & SIROVICH, L. 1992 Coherence and chaos in a model of turbulent boundary layer. *Phys. Fluids* A **4**, 2855–2874.